Second International Symposium on Marine Propulsors
smp'11, Hamburg, Germany, June 2011

Evaluation of the Propeller Hull Vortex Using a RANS Solver

Jussi Martio[1], Tuomas Sipilä[1], Antonio Sanchez-Caja[1], Ilkka Saisto[1],Timo Siikonen[2]

[1]VTT Technical Research Centre of Finland
[2]Aalto University

ABSTRACT

The appearance of the propeller hull vortex (PHV) has been investigated using the FINFLO RANS solver. This specific phenomenon occurs when solid surfaces placed in the neighbourhood of the propeller prevent the natural flow contraction resulting from the local flow acceleration. As the propeller blades near the solid surfaces may not obtain enough mass flow from the inlet – i.e., the propeller is starved of water - the flow may reverse locally so that water is sucked from the outlet. The small tip clearance combined with the low advance number as well as the geometry of the solid surfaces may affect the inception of the PHV.

Time-dependent computations were carried out at seven advance numbers. During the analysis of the results, several quantities were examined to detect the inception of the PHV. Streamlines were found to be the best technique to trace the vortices from an extremely complex flow field. The flow patterns on the flat plate were compared to published experimental observations using the limiting streamlines along the plate. Flow patterns similar to those discovered in the experiments were also obtained by RANS simulations, so the RANS method is able to predict the occurrence of the PHV at least on a qualitative level.

Keywords

Propeller-Hull Vortex, URANS

1 INTRODUCTION

Propeller-hull vortex (PHV) cavitation is a specific type of cavitation related to a stationary vortex between the propeller tip and the hull. The favourable conditions for the generation of the PHV are typically low advance numbers J, small clearance between the blade tip and the hull surface, and hull geometry. Flat plate geometry is presumed to produce more favourable conditions for the PHV than curved geometry (Carlton 2007). Traditionally, PHV cavitation has been studied by means of experimental modelling and full-scale observations.

The PHV phenomenon was first reported by Huse (1971). Four hypotheses were introduced as theoretical groundings for PHV cavitation. These hypotheses included the starting vortex, the vortices created by the shear flow in the wake field, the vortices created in other regions of the flow field, and the so-called pirouette effect. The pirouette effect emerges as the propeller works in a loaded condition and the tip clearance is small. This may result in situations where the blade's suction side gets starved of water. The pirouette effect was considered to be the dominant source for the inception of the PHV.

A more systematic investigation was carried out by Sato et al (1986). The procedure included experiments with six model propellers. A flat plate representing the hull surface was located above the propeller. The tip clearance was altered by moving the propeller vertically. Air bubbles were injected into the flow field in order to visualize the streamlines on the plate.

According to the observations, the flow patterns were classified into six specific categories, as described in Fig. 1. First, the air bubbles are moving uniformly to the downstream for the plate located far enough away from the propeller (Non-reverse flow). Once the plate approaches the blade tips, the flow starts occasionally to reverse. Still, no vortex is generated under this pattern (No-vortex reverse).

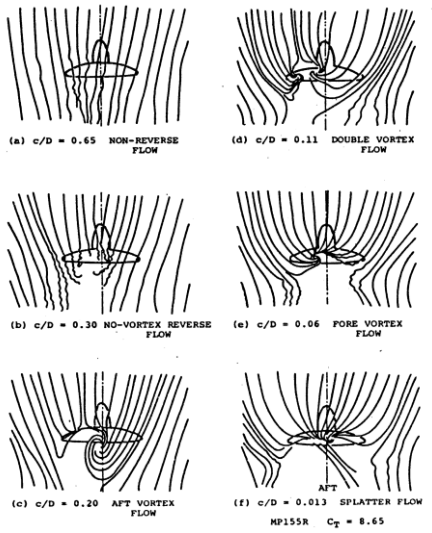

Figure 1: Bubble trajectories on the plate as tip clearance ratio c/D is varied (Sato et al 1986)

At the next stage, the reverse flow becomes stable and a vortex can be detected just above the propeller. This flow pattern is classified as the 'Aft vortex flow' situation. For right-handed propellers this specific vortex is rotating in a clockwise direction. As the c/D-ratio is decreased to a magnitude of 0.11, a 'Double vortex flow' flow field can

be detected. Two separate vortices are originated from the plate so that finally they are located side by side as shown in Fig. 1. A counter-clockwise vortex located on the port side of the clockwise rotating vortex is generated so that the flow image is no longer symmetrical with respect to the centreline. The instantaneous flow pattern actually looks like a vertical section of a mushroom.

The 'Fore vortex flow' situation emerges as the counter-clockwise vortex in this case moves close to the clockwise vortex. Finally, the vortices unite once the counter clockwise vortex absorbs the clockwise vortex.

The last flow pattern is achieved at c/D=0.013. This specific phenomenon was called the 'Splatter flow'. A strong jet flow is formed downstream from a point just above the propeller tip, as the blade is very close to the flat plate. A counter-clockwise vortex is generated on the starboard side of the jet flow. This particular vortex was specified as the 'splatter vortex'.

In Fig. 2, the different flow patterns are shown as a function of tip clearance ratio c/D and load factor C_T

$$C_T = \frac{8 \cdot T}{\pi \rho D^2 U^2} = \frac{8 \cdot K_T}{\pi J^2} \qquad (1)$$

where J denotes the advance number, T is the thrust, ρ is the density, D is the propeller diameter, U is uniform velocity, and K_T is the thrust coefficient. The suction limit and the vortex limit are drawn to separate 'Non-vortex flow', 'No-vortex reverse flow' and 'Aft vortex flow' from each other as explained.

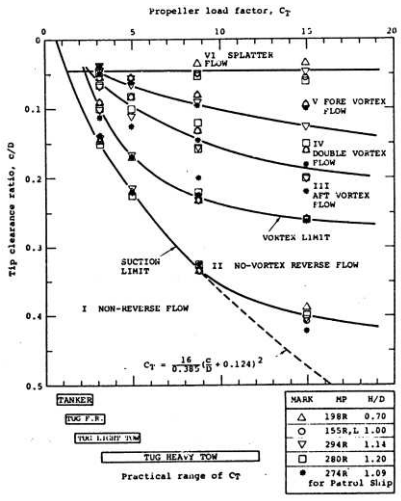

Figure 2: Flow patterns on the plate as a function of c/D and C_T (Sato et al 1986)

2 NUMERICAL METHOD

The flow simulation in FINFLO is based on the solution of the RANS equations by the pseudo-compressibility method. FINFLO solves the RANS equations by a finite volume method. The solution is extended to the wall and is based on approximately factorized time integration with local time stepping. The code uses either Roe's flux difference splitting or Van Leer's flux vector splitting for compressible flows and an upwind-based scheme for incompressible flows. In the latter case, the pressure is centre differenced and a damping term is added via a convective velocity. A multi-grid method is used for the acceleration of convergence. Solutions on coarse grid levels are used as the starting point for the calculation in order to accelerate convergence. For the time-accurate computations the interface between the rotating propeller grid blocks and the surrounding stationary blocks is treated using a sliding mesh technique, where the grid lines across the block interface are discontinuous. The solution for a block is interpolated using the solution in the neighbouring block. A mass-conserving interpolation is made between the connecting blocks at every time step. A detailed description of the numerical method including discretization of the governing equations, solution algorithm, etc. can be found in Sanchez-Caja et al (1999, 2000). Chien's k-epsilon turbulence model was used in the calculation.

Unsteady flows can be approximated using mixing plane and quasi-steady methods. In the mixing plane approach, the flow quantities for both the rotating and non-rotating blocks are circumferentially averaged on both sides of the common interface and then transferred to the ghost cells as boundary values. In the quasi-steady approach, the rotating and non-rotating blocks are connected without any averaging process. The simplified approaches may give sensible results when the interaction between the rotating and stationary domains is weak. For axial flows, even though the velocities everywhere are expressed in inertial coordinates, the flow disturbances are convected using different reference frames on the blocks at each side of the interface. The transition of the flow at the interface should be smooth without interferences of solid boundaries located nearby. In this investigation, a time-accurate approach was considered more appropriate to avoid interference of the flat plate.

FINFLO is also extended to model two-phase flows together with the cavitation model. The cavitation model is based on either Merkle's or Kuntz's mass transfer model (Sipilä et al 2009). The cavitation model is not applied in the present study.

3 CALCULATIONS

3.1 Propeller and grid specifications

The INSEAN E779a propeller was selected as the reference case for the study. The main characteristics of the model propeller are given in Table 1, while the surface grid of the propeller is shown in Fig. 3.

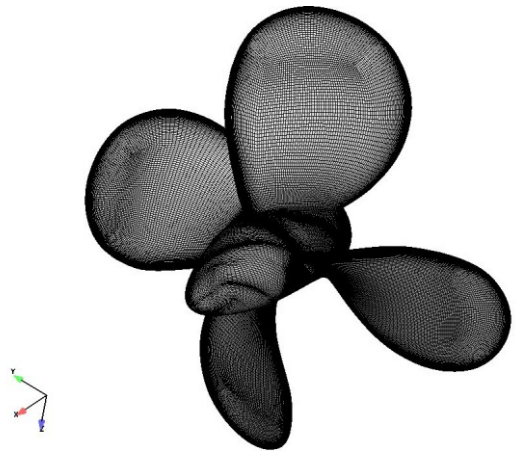

Figure 3: The schematic view of the INSEAN E779A propeller

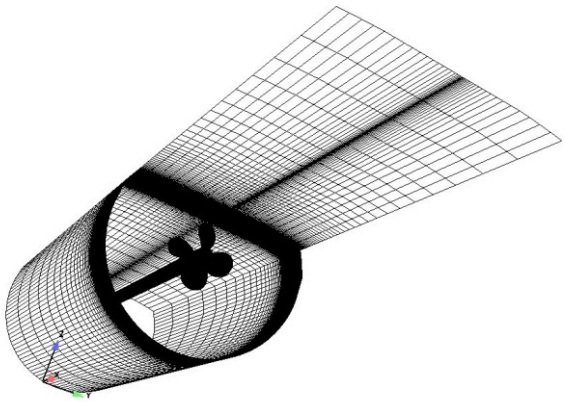

Figure 4: Schematic view of the asymmetrical grid

Table 1: Basic data of the INSEAN E779A model propeller

Propeller diameter D	227.27 mm
Number of blades	4
Rotation	Right-handed
Pitch ratio P/D	1.1

The flat plate was located at a given distance from the propeller tip. The grid configuration is shown in Fig. 4. The main parameters of the computation are presented in Table 2.

Table 2: Main parameters used in the study (time-accurate computation)

Number of elements	~1.1 million
Tip clearance c/D	0.157
Advance numbers time accurate	0.050, 0.099, 0.249, 0.326, 0.433, 0.532, 0.606
load factor C_T (exp.)	2.0, 2.9, 5.0, 10..0, 18.6, 132.0,. 531.7
propeller rotational rate (rps)	11.8
time step [s]	0.0001177

3.2 Time accurate computations

The computations were started with the quasi-steady approach. Once sufficient convergence was reached in the quasi-steady solution, the computation was continued in a time-accurate manner.

Examples of convergence histories of chosen quantities are presented in Fig. 5. The quasi-steady computation was stopped after approximately 20,000 iterations.

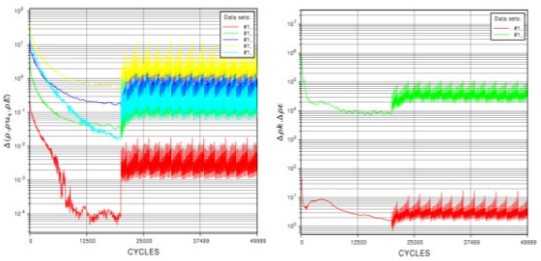

Figure 5: Example of convergence histories of the computations for the J=0.099. From left to right: L2 norms for the momentum residuals and L2 norms for k/e residuals

4 FLOW ANALYSIS

4.1 Analysing process

The most difficult part of the analysis was the visualisation of single vortices, which was a consequence of the complexity of the global flow field. Such complexity grows as the advance number of the propeller decreases. In other words, an individual vortex can be quite difficult to isolate from the global flow field. The vortices of interest are not stable, but strongly time-dependent. The size of the vortex compared to the global flow field can also be considered minimal.

The propeller-hull vortices were traced first by the pressure and velocity fields. Both absolute and relative velocities were used in this process. Furthermore, the vorticity isosurfaces were also displayed in order to detect possible PHV formation. All these quantities were found to be inconvenient for visualisation purposes, mainly because the suitable range for the specific quantity was found to be too sensitive to be selected properly.

A more convenient technique to display the PHV formation was to detect the limiting streamlines on the plate in a similar manner as sketched in Fig. 1. The origin of the PHV can be explored with the streamlines as well as its general shape.

The most detailed information about the structure of the flow pattern was obtained by searching the location of PHV with the limiting streamlines and using the instantaneous location of the vortex as the origin of the streamlines in the 3D-flow field. This technique also reveals whether or not the PHV is attached to the propeller blades.

4.1 Results

A summary of the findings is shown in Fig. 6. In principal, the flow should follow the patterns illustrated in Fig. 2 with c/D=0.157 for each C_T. According to Fig. 3, the flow should remain as a 'Non-reverse flow' at a C_T value of about ~3. This is illustrated in Figs. 6a and 6b, since the flow field remains uniform with C_T=2.0 but can be categorised as a 'No-vortex reverse flow' with a load factor magnitude of 2.9. The flow starts to swing to the port side of the propeller; still a distinct vortex cannot be isolated from the flow field.

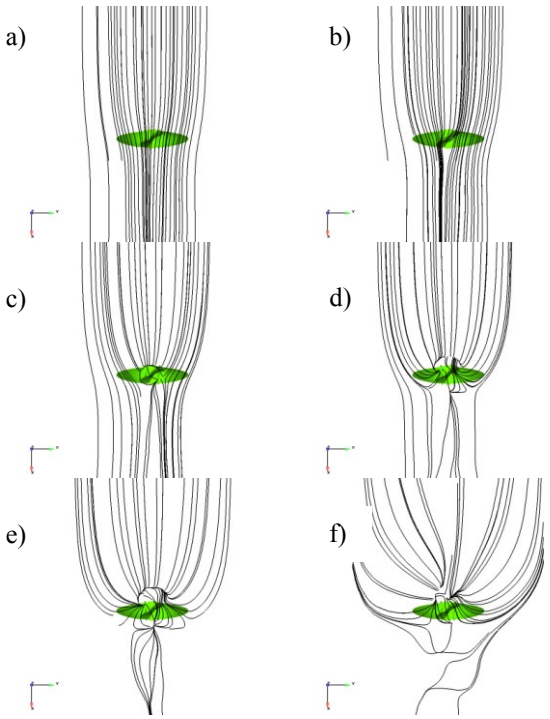

Figure 6: From left to right and top to bottom: The limiting streamlines on the plate with advance numbers 0.606, 0.532, 0.433, 0.326, 0.249, and 0.050. The corresponding load factors are 2.0, 2.9, 5.0, 10.0, 18.6 and 531.5. The positive x-axis points in the downstream direction

The 'Aft vortex flow' situation should emerge once the load factor reaches an approximate magnitude of 5. The limiting streamlines for this specific situation are shown in Fig. 6c. Clearly, a distinguished vortex is located just between the propeller and the plate. Once the loading is increased so that C_T reaches a value of 10.0, the 'Double vortex flow' condition appears. This is also demonstrated in Fig. 6d. Furthermore, the same pattern is even clearer with C_T=18.6. Finally, an instantaneous 'Fore vortex flow' situation emerges as the load factor is set to a magnitude of over 130. On average, the evaluated flow patterns follow the experimental observations very well. The suction and vortex limits defined by (Sato et al 1986) are produced reasonably well by the RANS method.

The limiting streamlines produced for four rotation angles are presented in Fig. 7 at advance number J=0.433. It may be concluded that the origin of the vortex remains quite steadily on the flat plate, but the form of the vortex changes as the blades encounter the vortex.

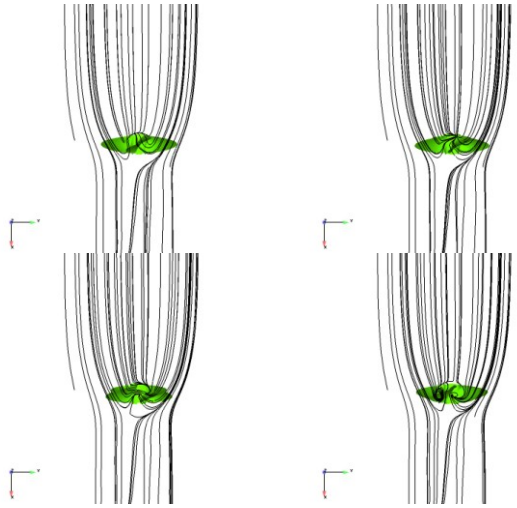

Figure 7: From left to right and top to bottom: The limiting streamlines on the plate with propeller rotation angles 0 deg, 25 deg, 40 deg and 70 deg. The advance number J=0.433. 0 deg refers to the blade at the 12 o'clock position

The computed K_T as a function of the propeller rotation angle is presented in Fig. 8. The oscillation of the thrust increases as the advance number is decreased. On the other hand, the evaluated time-averaged thrust coefficient remains almost constant in the advance number range 0.050 to 0.099. Also, small phase shifts in oscillations can be noticed between these advance numbers. At all advance numbers, the force and moment oscillations take place at the blade passing frequency corresponding to 90 deg rotation.

The oscillation amplitudes of K_T reduce significantly between advance numbers 0.249 and 0.326, as presented in Fig. 8. Still, both situations produce the 'Double vortex flow' condition, as shown in Figs. 6d and 6e, on the flat plate. Fig. 9 shows a more detailed illustration of the structure of the PHV. The 'Double vortex flow' formation with two distinct vortices is detected at J=0.249. The vortices rotating in the clockwise and counter-clockwise directions are interacting both with the blades and the tip vortices, depending on the propeller rotation angle. Furthermore, in this particular case, the vortices are also attached to the low-pressure region near the leading edge.

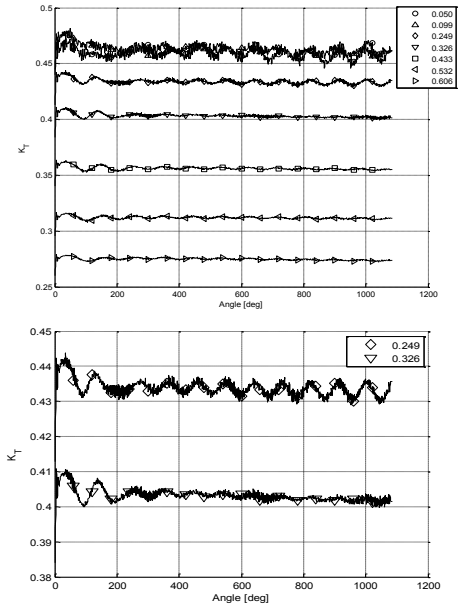

Figure 8: Top: The thrust coefficient K_T for the time-accurate computations as a function of rotation angle for all calculated advance numbers. Below: The oscillation of K_T for cases J=0.249 and J=0.326

As the loading on the propeller is decreased, that is, the advance number is increased to 0.326, the propeller-hull vortices do not seem to impinge on the blades. This is the probable explanation also why the fluctuation of the thrust coefficient strongly reduces between these advance numbers.

Finally, the vortex structures of the 'Aft vortex flow'-condition are studied in Fig. 11. The 'Vortex limit' was defined to separate the 'Aft vortex flow' and the 'No-vortex reverse flow' -situations from each other.

The traced streamlines at J=0.433 illustrate that also for this case the generated vortices emerging from the plate do not interact with the blades at any position. That is, the streamlines denoted with red colour are presumably affected by the tip vortices, but they do not impinge on the blades for any time step. Furthermore, the 'Double vortex flow' -situation is formed at the propeller rotational angle 70 deg. In this particular case, the vortices bypass the blades towards the downstream direction.

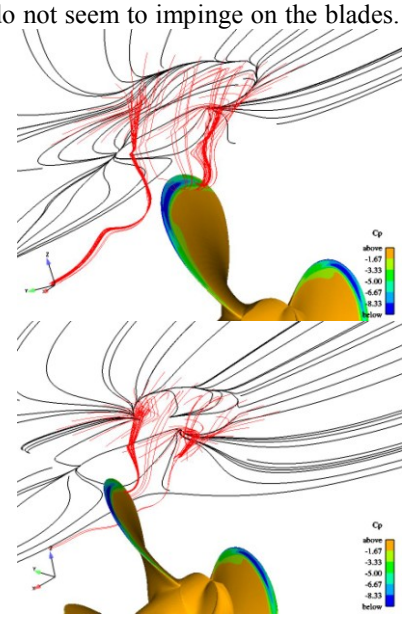

Figure 9: Top: the distribution of C_P on the suction side and streamlines with propeller rotation angle 0 deg. Below: the same for rotation angle 25 deg. The advance number is J=0.249

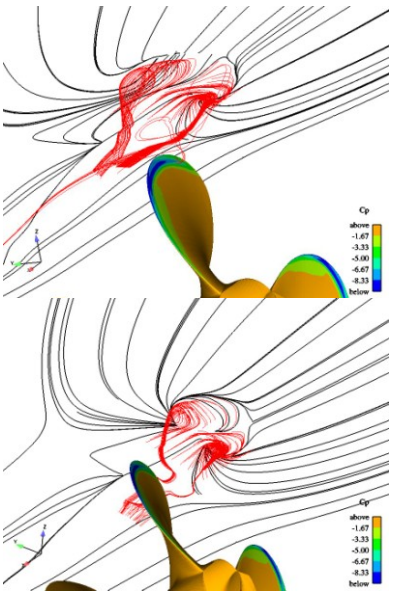

Figure 10: Top: the distribution of C_P on the suction side and streamlines with propeller rotation angle 0 deg. Below: the same for rotation angle 25 deg. The advance number is J=0.326

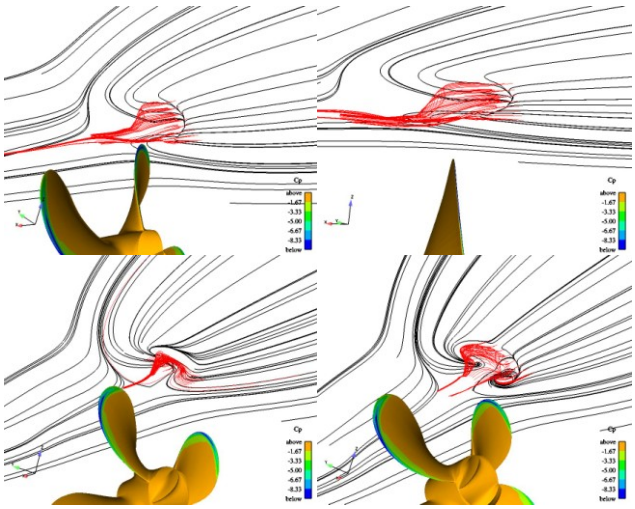

Figure 11: From left to right and top to bottom: the streamlines and the distribution of CP on the suction side with propeller rotation angles 0 deg (both top figures), 40 deg and 70 deg. The advance number is J=0.433

5 CONCLUSIONS

The fundamental mechanisms causing the propeller-hull vortex were modelled using the time-accurate RANS solver. Both steady-state and time-accurate approaches were utilised in the investigations.

The parameters affecting the strength of the PHV are blade loading and the tip clearance. The present computations were carried out using seven separate advance numbers and keeping the tip clearance constant.

The basic phenomena related to the so-called pirouette effect were detected at least with qualitative accuracy. As the tip clearance between the propeller blade tip and the wall is decreased, the blade's suction side does not obtain enough quantity of water from the inlet side. That is, water is also sucked from the downstream, causing the pirouette effect and the finally PHV inception.

The detection and measurement of the pirouette effect's strength were found to be major issues. Several flow quantities were tested, and finally, the limiting streamlines on the flat plate were found to be the most appropriate method of tracing the vortices. Once the location of the vortex or vortices was determined on the plate, a set of streamlines departing from this region could be created. This technique allowed the structure of vortex mechanism to be studied in a more detailed manner. Unfortunately, this technique does not provide any specific method to evaluate the strength of the vortex.

The flow patterns divided into six categories by (Sato et al 1986) were simulated and the agreement between the experimental observations and the results produced by the RANS method was considered to be satisfactory. The time-dependent phenomena were also reproduced reasonably well. It could be stated that the time-accurate viscous flow solver was able to predict the occurrence of the propeller-hull vortex on a qualitative level reasonably well. The detailed analysis of the flow structure also revealed that before PHV inception, a vorticial structure can be seen in the vicinity of the plate. In this initial situation, the vortex is not yet impinging on the blade.

Since the fundamental mechanisms causing the PHV can be modelled at least with some accuracy using the RANS method, the use of cavitation models would be the next step to improve the simulations at full scale. Also, the combined method using the vorticity, the helicity, or the mass flow together with the streamlines could be tested in the future to detect the 'pirouette effect' and to measure the strength of the PHV.

ACKNOWLEDGMENTS

This work has been was conducted in VIRKOOT-project sponsored by TEKES, the Finnish Funding Agency for Technology and Innovation. The authors are indebted to Dr. Jaakko V. Pylkkänen, who proposed PHV inception as a topic for CFD research before his retirement.

REFERENCES

Carlton, J. (2007). Marine Propellers and Propulsion. 2nd ed.

Huse. (1971) 'Propeller-Hull Vortex Cavitations'. Norw. Ship Model Exp. Tank Publ. **106**, May 1971.

Sato, R. et al. (1986). 'Observation of Flow on a Horizontal Flat Plate above a Working Propeller and Physics of Propeller-Hull Vortex Cavitation'. Proceed. Internat. Symposium on Propeller and Cavitation, Wuxi, China.

Sánchez-Caja, A., Rautaheimo, P., Salminen, E. & Siikonen, T. (1999). 'Computation of the Incompressible Viscous Flow around a Tractor Thruster Using a Sliding Mesh Technique'. Proceedings of the 7th International Conference in Numerical Ship Hydrodynamics, Nantes, France.

Sánchez-Caja, A., Rautaheimo, P. & Siikonen, T. (2000). 'Simulation of Incompressible Viscous Flow Around a Ducted Propeller Using a RANS Equation Solver'. 23rd Symposium on Naval Hydrodynamics, Val de Reuil, France.

Sipilä, T. et al. (2009). 'Cavitating Propeller Flows Predicted by RANS Solver with Structured Grid and Small Reynolds Number Turbulence Model Approach'. Proceedings of 7th International Symposium on Cavitation.